CHEMISTRY
A EUROPEAN JOURNAL

DOI: 10.1002/chem.200701592

Preparation and Characterization of a Microcrystalline Non-Heme $Fe^{III}(OOH)$ Complex Powder: EPR Reinvestigation of $Fe^{III}(OOH)$ Complexes—Improvement of the Perturbation Equations for the *g* Tensor of Low-Spin Fe^{III}

Marlène Martinho, Pierre Dorlet,* Eric Rivière, Aurore Thibon, Caroline Ribal, Frédéric Banse,* and Jean-Jacques Girerd[a]

Abstract: The first example of a microcrystalline powder of a synthetic low-spin (LS) mononuclear $Fe^{III}(OOH)$ intermediate has been obtained by the precipitation of the $[Fe^{III}(L_5^2)(OOH)]^{2+}$ complex at low temperature. The high purity of this thermally unstable powder is revealed by magnetic susceptibility measurements. EPR studies on this complex, in the solid state and also in frozen solution, are reported and reveal the coexistence of two related $Fe^{III}(OOH)$ species in both states. We also present a theoretical analysis of the *g* tensor for LS Fe^{III} complexes, based on new perturbation equations. These simple equations provide distortion-energy parameters that are in good agreement with those obtained by a full-diagonalization calculation.

Keywords: EPR spectroscopy · hydroperoxo · iron · microcrystalline powders · perturbation theory

Introduction

Mononuclear low-spin (LS) $Fe^{III}(OOH)$ species have been identified as intermediates in the activation of O_2 by natural systems, such as heme monooxygenases (e.g., Cytochromes P450)[1] or the antitumor drug bleomycin.[2] Intensive studies have been dedicated to modeling these intermediates, and we[3] and others[4] have been able to prepare and identify synthetic non-heme $Fe^{III}(OOH)$ complexes. In general, these intermediates are obtained by the addition of H_2O_2 to Fe^{II} complexes prepared with hexa-, penta-, and tetradendate aminopyridine ligands (see Scheme 1)[3,4] and have been characterized by several techniques, in particular, EPR and resonance Raman spectroscopy. Apart from two cases,[5,6] $Fe^{III}(OOH)$ species exhibit LS Fe^{III} EPR features and their vibrational characteristics indicate an end-on coordination mode for the hydroperoxo ligand.[7,8] These complexes have always been prepared and studied in solution and no crystal structures have been reported to date.

Previously, we reported the preparation of the complex $[Fe^{III}(L_5^2)(OOH)]^{2+}$[8] (see Scheme 1 for the structure of L_5^2) in solution and its EPR analysis in the framework of the Griffith–Taylor model,[9,10] which has been extensively used for LS Fe^{III} EPR investigations and was recently reviewed in the literature.[11–13] Herein, we report the isolation of LS $[Fe^{III}(L_5^2)(OOH)](PF_6)_2$, which is the first example of a microcrystalline powder for such a thermally unstable intermediate. The temperature-dependent magnetic susceptibility and the EPR properties of this complex were studied and are reported herein. The EPR signal was analyzed in the solid state and in a frozen solution and revealed the presence of two species in both cases. The *g* tensor of these species, which was measured in the well-resolved solution spectrum, was investigated by using new and improved perturbation equations. The nature of these two species is also discussed herein.

[a] Dr. M. Martinho, Dr. P. Dorlet, Dr. E. Rivière, Dr. A. Thibon, Dr. C. Ribal, Dr. F. Banse, Prof. J.-J. Girerd
Institut de Chimie Moléculaire et des Matériaux d'Orsay
UMR CNRS 8182
Equipe de Chimie Inorganique
Université Paris Sud
91405 Orsay Cedex (France)
Fax: (+33) 169-154-754
E-mail: pierre.dorlet@cea.fr
fredbanse@icmo.u-psud.fr

Supporting information for this article is available on the WWW under http://www.chemeurj.org/ or from the author.

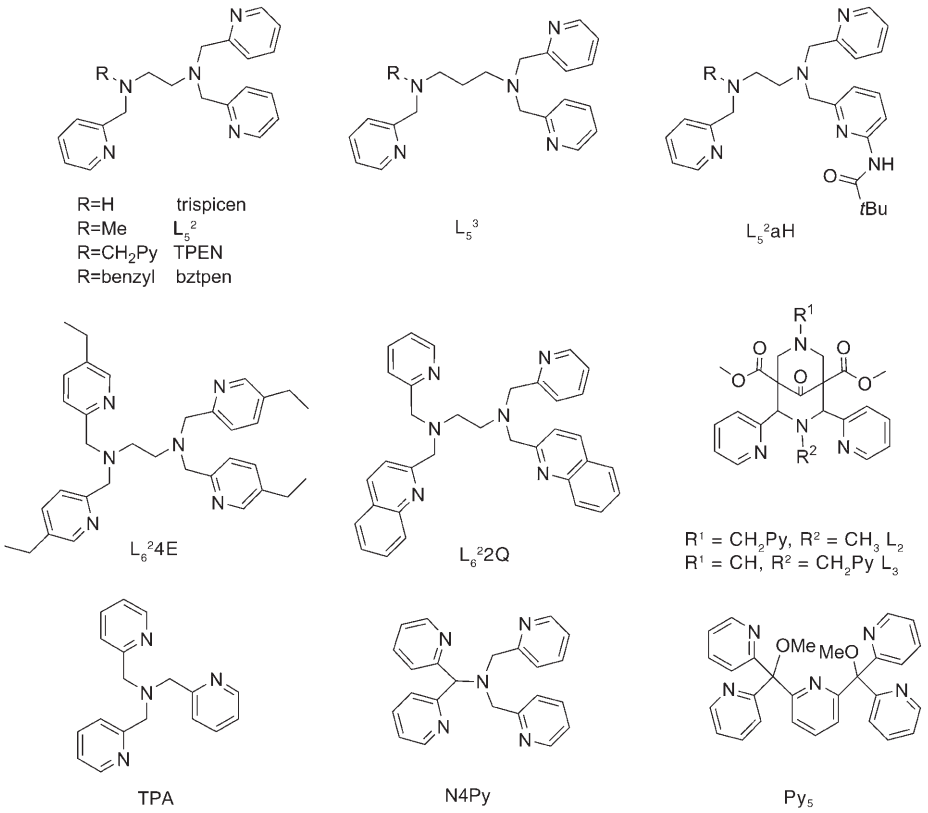

Scheme 1. Ligands that have allowed the formation of LS $Fe^{III}(OOH)$ complexes.

Results

Addition of a 100-fold excess of H_2O_2 to a solution of $[Fe^{II}Cl(L_5^2)]PF_6$ in methanol leads to the formation of the complex $[Fe^{III}(L_5^2)(OOH)]^{2+}$, as previously described.[14] This purple species absorbs at 537 nm ($\varepsilon = 1000\,M^{-1}cm^{-1}$).[8] The 9 GHz EPR spectrum of the solution, recorded in methanol, is shown in Figure 1B. This spectrum is better resolved than those previously obtained for the same complex or those reported for related species under slightly different conditions,[8] that is, with different mixtures of solvents (see the Supporting Information). Several features can be distinguished from the spectrum, which could be due to either hyperfine couplings or a mixture of species with different g values. Because the Zeeman effect depends linearly on the magnetic field, whereas hyperfine splitting is field-independent, we recorded the EPR spectrum at 34 GHz (Figure 1C) to distinguish between these two possibilities. The comparison between Figure 1B and C shows that the g values are the same in the spectra recorded 9 and 34 GHz, which demonstrates the presence of distinct species.

A weak signal, with g values of 2.33, 2.14, and 1.94, is also observed (Figure 1B). It is identical to the spectrum obtained when only one equivalent of H_2O_2 is added to a solution of $[Fe^{II}Cl(L_5^2)]PF_6$ in methanol or for an equimolar mixture of L_5^2 and $Fe^{III}(NO_3)_3$ in methanol (Figure 1A). This weak signal is, therefore, attributed to the $[Fe^{III}(L_5^2)(OMe)]^{2+}$ complex. The main signal mostly arises from the presence of two species and could be simulated by superimposing two sets of g values ($g_{1A}=2.215$, $g_{2A}=2.150$, $g_{3A}=1.973$; and $g_{1B}=2.184$, $g_{2B}=2.123$, $g_{3B}=1.973$) for two species (denoted A and B, respectively) by using the convention $g_1 > g_2 > g_3$. The best simulations of the 9 and 34 GHz data are displayed in Figure 1 (gray lines), along with the experimental data (black lines). The relative proportions of the various species for the calculated 9 GHz spectrum are 57% for species A, 40% for species B, and 3% for the methoxy complex $[Fe^{III}(L_5^2)(OMe)]^{2+}$. For the calculated 34 GHz spectrum, the relative proportions are 56% for species A and 44% for species B. The amount of methoxy species detected in the spectra varied from sample to sample, but was always very low ($\leq 5\%$). The relative proportions of A and B did not vary significantly from sample to sample or as a result of slight changes to the preparation conditions (e.g., addition of small amounts, typically 10%, of water, glycerol, ethanol, etc.), and were estimated to be roughly in the ratio

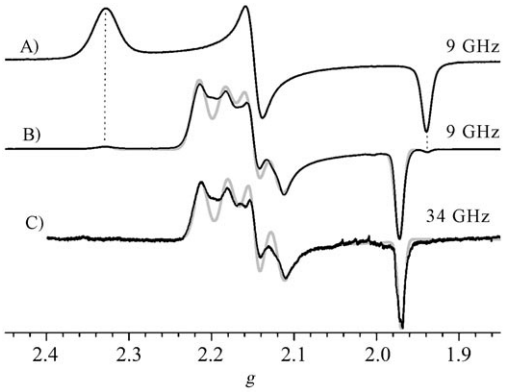

Figure 1. Experimental (black) and calculated (gray) EPR spectra of A) an equimolar solution of L_5^2 and $Fe^{III}(NO_3)_3{\cdot}9H_2O$ in methanol, B) and C) $[Fe^{II}Cl(L_5^2)]^+$ in methanol after the addition of H_2O_2 (100 equiv) at room temperature. Experimental conditions: A) microwave frequency = 9.37425 GHz, modulation amplitude = 0.1 mT, microwave power = 1.00 mW, $T = 100$ K; B) microwave frequency = 9.38037 GHz, modulation amplitude = 0.1 mT, microwave power = 2.00 mW, $T = 90$ K; and C) microwave frequency = 33.97047 GHz, modulation amplitude = 0.8 mT, microwave power = 2.31 mW, $T = 100$ K.

60:40. The remaining small contribution from other species has been ignored in this study. The *g* values obtained for A and B are similar to those reported for LS non-heme Fe^{III}-(OOH) in the literature.[3,4] Therefore, we propose that both species A and B are LS Fe^{III}(OOH) complexes with the generic formula $[Fe^{III}(L_5^2)(OOH)]^{2+}$.

Previously, Wada and co-workers prepared a high-spin (HS) Fe^{III}(OOH) complex as a powder, but the solid was not characterized by spectroscopy.[5] By adding diethyl ether to a solution of $[Fe^{III}(L_5^2)(OOH)]^{2+}$ and $NaPF_6$ in methanol, we were able to obtain a purple powder. The 9 GHz EPR spectrum of this purple powder (as a suspension in diethyl ether) was recorded and is shown in Figure 2.

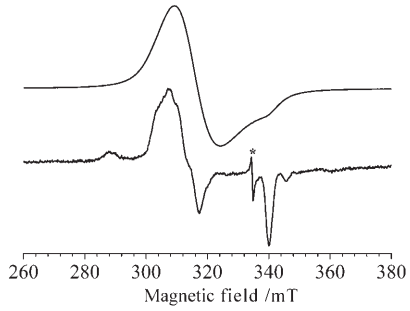

Figure 2. Top: EPR spectrum of a frozen suspension of $[Fe^{III}(L_5^2)$-$(OOH)](PF_6)_2$ in diethyl ether. Experimental conditions: microwave frequency = 9.38180 GHz, modulation amplitude = 0.1 mT, microwave power = 2.01 mW, and T = 90 K. Bottom: EPR spectrum of a frozen suspension of $[Fe^{III}(L_5^2)(OOH)](PF_6)_2$ in diethyl ether, diluted with $[Zn^{II}$-$(L_5^2)]Cl_2$, (mol/mol = 0.5:100). Experimental conditions: microwave frequency = 9.38096 GHz, modulation amplitude = 0.1 mT, microwave power = 0.02 mW, and T = 5 K. *: Instrument artifact.

The spectrum is characterized by a broad axial powder pattern over the range of *g* values observed in solution for the Fe^{III}(OOH) species. As expected, the 34 GHz spectrum was better resolved with respect to *g* anisotropy (data not shown). The broadening of the spectrum is a well-known feature for powders and arises from spin–spin interactions between paramagnetic species in close proximity. To improve the resolution of the spectrum, we obtained a magnetically diluted powder by co-precipitating the iron complexes with a diamagnetic zinc complex at various dilution ratios (iron complex = 10, 1, and 0.5 %). The EPR spectrum linewidth narrowed with increasing dilution. Figure 2 shows the best-resolved 9 GHz spectrum. Although it is still slightly broader compared with the solution spectrum in methanol, features that correspond to species A and B are clearly distinguishable, along with a small amount of Fe^{III}(OMe) complex. Therefore, the powder that was precipitated contains the same complexes as initially observed in solution and is mostly constituted of Fe^{III}(OOH) species A and B. Note from the experimental spectra that A and B are present in similar relative amounts in the powder and the solution.

The temperature dependence of the magnetic susceptibility of the powder was measured by cyclically varying the temperature between 2 and 300 K. As shown in Figure 3,

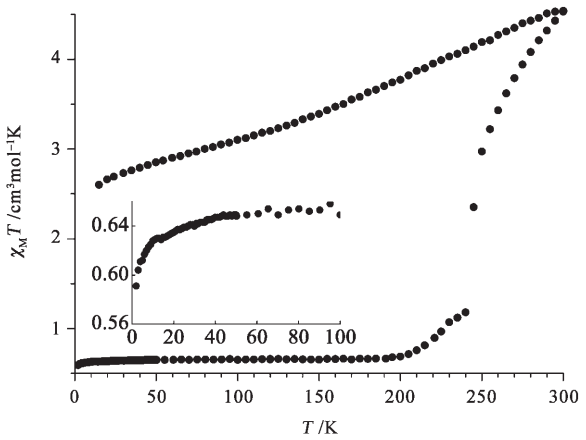

Figure 3. Plot of $\chi_M T$ as a function of T for the powder $[Fe^{III}(L_5^2)(OOH)]$-$(PF_6)_2$ between 2 and 300 K. Inset: The initial range between 2 and 100 K.

$\chi_M T$ is constant, with a value of 0.65 $cm^3 mol^{-1} K$ between 50 and 200 K. At higher temperatures, the $\chi_M T$ value increases and reaches a value of about 4.5 $cm^3 mol^{-1} K$ at 300 K. The behavior described above is not reversed when the temperature is lowered, which indicates the degradation of the sample above 200 K. This degradation is also revealed by the color change of the sample from purple to yellow. For a LS complex, such as $[Fe^{III}(L_5^2)(OOH)](PF_6)_2$, a $\chi_M T$ value of 0.375 $cm^3 mol^{-1} K$ is predicted by the Curie law, assuming $g = 2$. The measured value of 0.65 $cm^3 mol^{-1} K$ can be attributed to contamination by the presence of a HS ($S = {}^5/_2$) Fe^{III} species, as seen in the EPR spectra (data not shown). This hypothesis is supported by the decrease in the $\chi_M T$ curve below 50 K, which is induced by the zero field splitting of HS Fe^{III}. By considering a HS complex with a typical $\chi_M T$ value of 4.375 $cm^3 mol^{-1} K$, the amount of contamination was estimated to be only 6 %. These results indicate that the purple powder, prepared as described above, contains the two Fe^{III}(OOH) species A and B with high purity.

In the light of the better-resolved EPR spectra obtained for $[Fe^{III}(L_5^2)(OOH)]^{2+}$ in methanol, we recorded the EPR spectrum of some of our old and new Fe^{III}(OOH) complexes under the same conditions (Figure 4). In all complexes except $[Fe^{III}(L_5^3)(OOH)]^{2+}$, two powder patterns were necessary to fit the data. Note that L_5^3 is based on a propanediamine fragment, whereas the other ligands presented herein are based on an ethanediamine fragment (Scheme 1). We have previously observed a single powder pattern with the ligand L_5^2aH, for which we proposed a mixed N/O coordination sphere.[15] The sets of *g* values obtained by simulating the data are reported in Table 1.

Discussion

Basic features of LS Fe^{III} EPR spectra: It is known that the degeneracy of the ^2T ground state of LS Fe^{III} is lifted upon crystal-field distortion (defined by the parameters Δ and V; Figure 5) and spin-orbit coupling to give three Kramers dou-

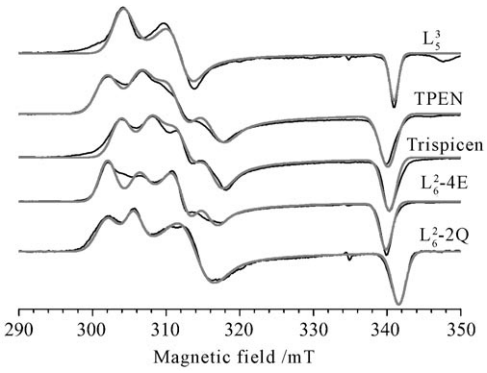

Figure 4. Experimental (black) and calculated (gray) X-band EPR spectra of some LS Fe^{III}(OOH) complexes. Experimental conditions: L_5^3: microwave frequency 9.38749 GHz, modulation amplitude 0.5 mT, microwave power 2.00 mW, 100 K; TPEN: microwave frequency 9.37911 GHz; modulation amplitude 1.0 mT; microwave power 0.03 mW, 100 K; trispicen: microwave frequency 9.37905 GHz; modulation amplitude 1.0 mT; microwave power 0.30 mW, 100 K; $L_6^2$4E: microwave frequency 9.38124 GHz; modulation amplitude 0.5 mT; microwave power 0.50 mW, 100 K; $L_6^2$2Q: microwave frequency 9.38545 GHz; modulation amplitude 0.25 mT; microwave power 2.00 mW, 100 K. For structures of the ligands, see Scheme 1.

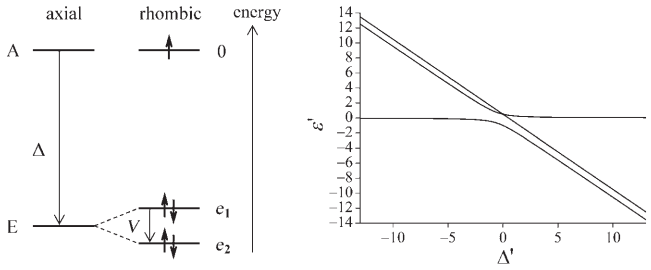

Figure 5. Energetic diagram showing the three occupied d orbitals for $S=\frac{1}{2}$ Fe^{III} complexes. Left: Δ represents the energy difference between the E and A orbitals, such that a negative value of Δ leaves the unpaired electron in the A orbital, as represented here. Right: energy of the three Kramers doublets as a function of the axial distortion parameter Δ′ ($V'=0$).

blets. In the simple case of axial distortion ($V=0$) and pure d orbital states, the energy of the doublets is represented in Figure 5. The energy of the lowest Kramers doublet in the reduced coordinate ($x'=x/\zeta$, in which ζ designates the spin-orbit coupling constant) is given by Equation (1):

$$\varepsilon' = \frac{-\Delta' - \frac{1}{2} - \sqrt{\left(\Delta' + \frac{1}{2}\right)^2 + 2}}{2} \quad (1)$$

For $\Delta'=0$, the splitting of the ^2T state under spin-orbit coupling is recognizable. Two extreme cases are physically distinct: 1) for large values of Δ′, the ground Kramers doublet is close to the first excited doublet and some orbital moment remains and 2) for large negative values of Δ′, the ground Kramers doublet is well separated from the excited doublets. This latter situation corresponds to an unpaired electron in a well-separated orbital with complete quenching of orbital momentum.

The corresponding g values for this doublet are given by Equations (2) and (3), in which g_e represents the free-electron g value.

$$g_\perp = \frac{g_e - 4\varepsilon'}{1+2\varepsilon'^2} \quad (2)$$

$$g_\parallel = \frac{g_e - 2\varepsilon'^2(2+g_e)}{1+2\varepsilon'^2} \quad (3)$$

Table 1. Results of g values and energy parameters obtained from perturbation theory and full diagonalization calculations for various LS Fe^{III}(OOH) complexes.

Ligand	Complex	Perturbations						Diagonalization					Ref.
		g_{max}[a]	g_{inter}[a]	g_{min}[a]	e'_1	e'_2	k	e'_1	e'_2	k	Δ′	V'	
L_5^2 (A)	**1**	2.215	2.150	1.973	−12.186	−8.462	0.900	−12.553	−9.039	0.963	−10.796	−3.514	this work
L_5^2 (B)	**2**	2.184	2.123	1.973	−12.189	−8.097	0.736	−12.421	−8.707	0.798	−10.564	−3.714	this work
L_5^2aH	**3**	2.23	2.16	1.96	−9.951	−6.892	0.785	−10.268	−7.481	0.861	−8.875	−2.787	[15]
L_5^3	**4**	2.206	2.150	1.967	−10.589	−7.678	0.782	−9.690	−7.585	0.851	−9.612	−2.676	this work
$L_6^2$4E (A)	**5**	2.219	2.147	1.972	−12.254	−8.182	0.887	−12.035	−8.521	0.951	−10.668	−3.119	this work
$L_6^2$4E (B)	**6**	2.187	2.123	1.972	−12.102	−7.909	0.730	−12.116	−8.131	0.793	−10.413	−3.790	this work
$L_6^2$2Q (A)	**7**	2.220	2.139	1.963	−12.713	−7.983	0.869	−10.954	−7.018	0.819	−9.280	−3.640	this work
$L_6^2$2Q (B)	**8**	2.194	2.129	1.963	−10.409	−6.880	0.659	−9.977	−7.384	0.732	−9.046	−3.087	this work
trispicen (A)	**9**	2.205	2.143	1.969	−11.218	−7.787	0.789	−11.669	−8.504	0.856	−9.959	−3.154	this work
trispicen (B)	**10**	2.176	2.119	1.969	−11.182	−7.512	0.652	−11.288	−8.504	0.718	−9.759	−3.233	this work
TPEN (A)	**11**	2.219	2.150	1.970	−11.664	−7.950	0.861	−12.048	−8.392	0.928	−10.265	−3.467	this work
TPEN (B)	**12**	2.186	2.120	1.970	−11.798	−7.559	0.694	−11.288	−8.504	0.759	−10.063	−3.773	this work
N4Py	**13**	2.16	2.11	1.98	−13.747	−9.388	0.740	−14.011	−10.003	0.794	−12.007	−4.008	[17]
Py_5	**14**	2.15	2.13	1.98	−12.00	−10.38	0.767	−12.498	−10.976	0.821	−11.737	−1.522	[18]
bztpen	**15**	2.22	2.18	1.97	−10.61	−8.66	0.943	−11.102	−9.237	1.010	−10.170	−1.865	[19]
TPA	**16**	2.19	2.15	1.96	−9.01	−7.09	0.666	−9.407	−7.702	0.742	−8.555	−1.705	[20]
L^2	**17**	2.19	2.13	1.96	−9.78	−6.66	0.625	−9.984	−7.286	0.700	−8.635	−2.698	[21]
L^3	**18**	2.18	2.12	1.95	−8.77	−5.81	0.516	−8.842	−6.467	0.599	−7.655	−2.375	[21]

[a] The g values obtained by simulation of the spectra shown in Figure 4 are given with an accuracy of 0.001. Other values are given as previously reported.

These expressions lead to signed values for g. However, only the absolute g values are determined in most experiments and will be dealt with in the rest of the paper (for discussions on the sign of the g values see, for example, references [11–13]). The absolute g values are represented in Figure 6 as a function of Δ'. For large negative Δ' values, g values are close to g_e, as expected. Figure 6 also shows g values for the rhombic case in which $V'=0.2$, as an example. The expressions for the g values for this case are given in the Supporting Information. The g values for the positive values of Δ' are much more sensitive to rhombicity than for the negative values of Δ'. The positive value of Δ' case is frequently encountered in LS heme systems,[11] whereas the negative value of Δ' case occurs in non-heme $Fe^{III}(OOH)$ model complexes.[3] In this latter case, which is of interest here and which will be dealt with in the rest of the paper, all of the g values are positive.

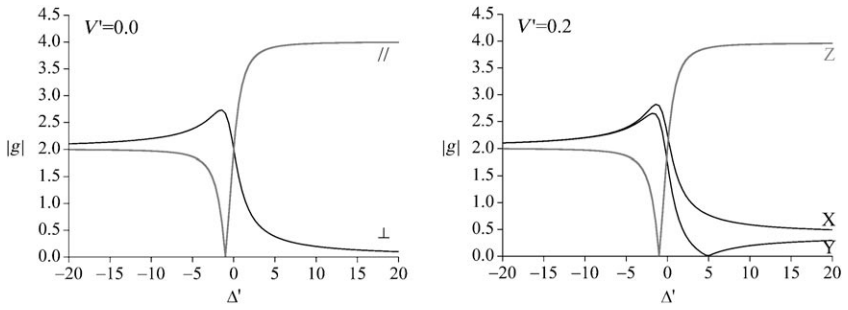

Figure 6. Representation of the absolute g values as a function of Δ', for the axial case (left) in which $V'=0.0$ and for the rhombic case (right) in which $V'=0.2$.

Perturbation theory: Neese et al.[16] give perturbation equations for the g values for an unpaired electron in a well-separated orbital ($\Delta<0$); this particular energetic situation for $Fe^{III}(OOH)$ complexes is shown in Figure 5. The expressions of the g values are shown in Equations (4) to (6), in which e_1 and e_2 represent the energy of the orbitals as defined in Figure 5 ($e_1=\Delta-V/2$ and $e_2=\Delta+V/2$):

$$g_{max} = g_e - \frac{2}{e'_1} \tag{4}$$

$$g_{int} = g_e - \frac{2}{e'_2} \tag{5}$$

$$g_{min} = g_e - \frac{1}{e'_1 e'_2} \tag{6}$$

From these equations, the order of magnitude of the energies of the doubly occupied orbitals relative to that of the singly occupied orbitals can be directly determined.

However, the g_{min} value computed from values of e_1 and e_2 calculated from g_{max} and g_{int} was found to be much closer to g_e than to the experimental values for g_{min} (Figure 7). It appears that the equation for calculating g_{min} is unsatisfactory, as noted by Neese et al.[16] In fact, for the axial case ($V'=0$, $e'_1=e'_2=\Delta'$), Equation (6) can be rewritten as: $g_{\parallel}=g_e-(1/\Delta'^2)$. However, the development of Equation (3) for large negative values of Δ' leads to $g_{\parallel}\approx 2-(3/\Delta'^2)$ (see the Supporting Information). Therefore, Equation (6) is incorrect because some second-order terms that should have been taken into account have been neglected. The treatment detailed in the Supporting Information yields perturbation Equation (7) for g_{min}:

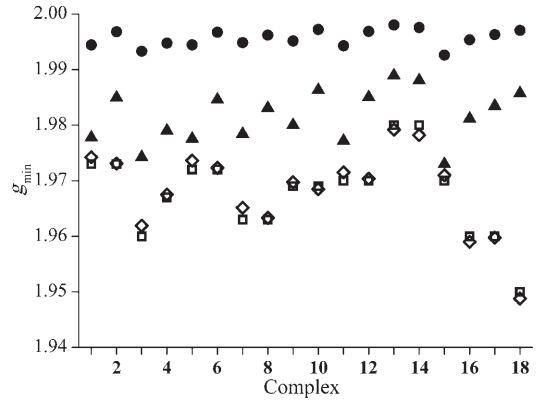

Figure 7. Graphical comparison of experimental and calculated values of g_{min} for the complexes listed in Table 1. □: Experimental values of g_{min}; ●: g_{min} values calculated from Equation (6); ▲: g_{min} values calculated from Equation (7), in which e'_1 and e'_2 were obtained from Equations (4) and (5); and ◇: g_{min} value calculated from Equation (13), in which Δ' was obtained from a diagonalization calculation.

$$g_{min} = \frac{g_e\left[1-{}^1\!/_4\left(\frac{1}{e'^2_1}+\frac{1}{e'^2_2}\right)\right]-\frac{1}{e'_1 e_2}}{1+{}^1\!/_4\left(\frac{1}{e'^2_1}+\frac{1}{e'^2_2}\right)} \tag{7}$$

The agreement between the experimental values and the perturbation values calculated by using Equation (7) is better (Figure 7), but the experimental value of g_{min} is still not exactly reproduced by this model. Indeed, only two parameters (e_1 and e_2) are used to account for three independent g values. To improve this model, the orbital reduction factor, k, was introduced as a third parameter. This parameter takes into account the covalence of the metal–ligand bonds.[11] This gives Equations (8)–(10):

$$g_{max} = g_e - \frac{2k}{e'_1} \tag{8}$$

$$g_{int} = g_e - \frac{2k}{e'_2} \tag{9}$$

$$g_{min} = \frac{g_e\left[1-{}^1\!/_4\left(\frac{1}{e_1'^2}+\frac{1}{e_2'^2}\right)\right]-\frac{k}{e_1'e_2'}}{1+{}^1\!/_4\left(\frac{1}{e_1'^2}+\frac{1}{e_2'^2}\right)} \quad (10)$$

These equations have been applied to several Fe^{III}(OOH) complexes from our lab and others. The energies and k values thus obtained are given in Table 1.

These results were compared to a full diagonalization calculation, which also took into account the orbital reduction factor (see the Supporting Information for the equations for the g values).[11] The results of the full diagonalization calculations are also reported in Table 1. The agreement for the energy values between the perturbation and the full diagonalization calculation is quite satisfactory. Indeed, the difference between these values is less than 10%, except in a few cases. The larger differences were recorded for $L_6^2$2Q (A), with disagreements of 15 and 13% for e_1' and e_2', respectively. For the k values, the results between both treatments are also in agreement within about 10%, except for TPA, L_2, and L_3, for which errors of 11, 11, and 15% are obtained, respectively. Therefore, to obtain relevant values for the orbital energies of the $S={}^1\!/_2$ Fe^{III}(OOH) complexes, the simpler perturbation equations [Eq. (8)–(10)] that directly link the g values to the energy parameters can be used, rather than a full diagonalization calculation.

In addition, we found that calculating g_{min} from the very simple Equation (13) (which is based on the axial case and assumes $k=1$) with the value of Δ' obtained by a full diagonalization calculation gave values that were in excellent agreement with the experimental measurements (Figure 7; the largest difference between experimental and calculated values is 0.11%). Reciprocally, this means that for LS Fe^{III}-(OOH) complexes, Δ' can be calculated directly from the experimental value of g_{min} by using Equation (13), and from this value k and V' are easily calculated from Equations (8) and (9). Therefore, in this case Equations (11) to (13) are the most useful:

$$g_{max} = g_e - \frac{2k}{\Delta' - (V'/2)} \quad (11)$$

$$g_{int} = g_e - \frac{2k}{\Delta' + (V'/2)} \quad (12)$$

$$g_{min} = 2 - \frac{3}{\Delta'^2} \quad (13)$$

Going back to the EPR spectra for this family of LS Fe^{III}-(OOH) complexes, we generally observe a mixture of two Fe^{III}(OOH) species, denoted A and B. A similar observation was made by Roelfes et al.[17] These two species exhibit g and calculated orbital energy values that are close to each other (Table 1), but the main difference is observed between the k values of the two species. In the complex with the ligand N4Py reported by Roelfes et al., one of the two species was largely predominant. They suggested that in the dominant complex, $[Fe^{III}(N4Py)(OOH)]^{2+}$, the projection of the hydroperoxo group onto the equatorial plane bisects the Fe–N bonds.[17] By analogy, the two close EPR signals we observe in our complexes could be attributed to two rotation isomers for A and B as illustrated in Scheme 2 for $[Fe^{III}(L_5^2)(OOH)]^{2+}$.

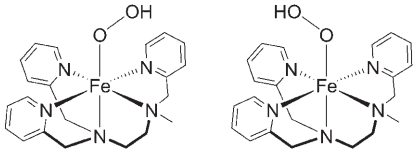

Scheme 2. Schematic representation of two rotation isomers of $[Fe^{III}(L_5^2)$-$(OOH)]^{2+}$. Left: The projection of the O–O bond in the equatorial plane bisects a pyridine-Fe-amine angle. Right: The projection of the O–O bond in the equatorial plane bisects a pyridine-Fe-pyridine angle.

Another obvious possibility would be that A and B are geometric isomers. That is, they may exhibit different configurations for the ancillary ligand, in which the hydroperoxo group is arranged *trans* to either a pyridine or an amine. This scenario could explain the change in the Fe–OOH covalent bond that is suggested by the change in the k value.[22] A more definite answer could be given by resolving the molecular structure of these intermediates with the help of single-crystal XRD analysis. The isolation and characterization of a microcrystalline powder of this complex, which is the central point of this paper, is the first step in that direction.

Conclusion

We have prepared a sample of a pure powder of $[Fe^{III}(L_5^2)$-$(OOH)](PF_6)_2$. The sample contains two closely related Fe^{III}(OOH) species, as shown by the results of EPR spectroscopy. A similar observation has been made for a series of related Fe^{III}(OOH) complexes in solution. Analysis of the g values by relevant perturbation equations indicates that both species have similar orbital-energy parameters. Therefore, we propose that the two species are geometric isomers. The assumption that the Fe^{III}(OOH) species exist as two isomers should be confirmed by single-crystal XRD analysis when it becomes possible.

A large amount of literature is dedicated to the theoretical analysis of the g values of LS Fe^{III} complexes. In the case of Fe^{III}(OOH) complexes, for which there is a large energy separation between the singly occupied molecular orbital and the other two populated d orbitals, we propose easy-to-handle perturbation equations that are compatible with a full diagonalization calculation. Validation of the theoretical model would necessitate direct experimental measurements of the energy parameters Δ and V.

Experimental Section

General: Electronic absorption spectra were recorded by using a Varian Cary 50 spectrophotometer equipped with a Hellma immersion probe and fiber-optic cable. For low-temperature experiments, a Thermo Haake CT90L cryostat was used.

EPR spectra were recorded at 9 and 34 GHz by using a Bruker ELEXSYS 500 spectrometer equipped with a continuous-flow Oxford E900 cryostat. Simulations of the EPR spectra were performed by using the XSophe Computer Simulation Software Suite.[23]

Magnetic susceptibility measurements were carried out by using a Quantum Design SQUID Magnetometer with an applied field of 1 kOe. The susceptibility data were corrected for diamagnetic contributions as deduced by using Pascal's constant tables.

Syntheses: Chemicals were purchased from Acros. Solvents were purchased from VWR and used without further purification. The preparation and handling of air-sensitive materials were carried out under an inert atmosphere by using standard Schlenk and vacuum-line techniques.

Ligand L_5^2 (Scheme 1) and $[Fe^{II}Cl(L_5^2)]PF_6$ were prepared according to previously described procedures.[24] The preparation of $[Fe^{III}(L_5^2)(OOH)](PF_6)_2$ was carried out by the addition of H_2O_2 (100-fold excess, 35% in water) to $[Fe^{II}Cl(L_5^2)]PF_6$ (2–3 mM in methanol) at room temperature to form the purple complex $[Fe^{III}(L_5^2)(OOH)]^{2+}$.[8,24] The reaction was monitored over time by using UV/Vis absorption spectroscopy. The solution was cooled to −64 °C before a cold, saturated solution of NaX (X = PF_6^-, ClO_4^-) in methanol was added to the mixture with stirring. Cold diethyl ether was then added, which resulted in a turbid solution and the formation of a purple precipitate. After stirring for several minutes, the precipitate was left to settle out and then it was filtered at low temperature, collected, and stored in liquid nitrogen until use. Note that the powder decomposes upon warming, therefore all equipment was cooled in liquid nitrogen before use.

For EPR purposes, we prepared a magnetically diluted powder of $[Fe^{III}(L_5^2)(OOH)](PF_6)_2$ in a diamagnetic host. An equimolar solution of L_5^2 and $ZnCl_2$ (typically 0.1 M) in methanol was prepared at room temperature. A solution of $[Fe^{III}(L_5^2)(OOH)]^{2+}$ in methanol was prepared separately at room temperature, according to a previously described procedure.[14] The room-temperature $Fe^{III}(OOH)$ solution was added to the solution that contained the Zn^{II} complex in various ratios of dilution. The mixture was then cooled to −60 °C to avoid decomposition of the $Fe^{III}(OOH)$ complex and a cold, saturated solution of $NaPF_6$ was added to the mixture. Cold diethyl ether was added to coprecipitate the Zn^{II} and $Fe^{III}(OOH)$ complexes. The pinkish-white powder was filtered at low temperature, collected, and stored in liquid nitrogen until use.

Acknowledgements

The authors thank the French program "Energie, Conception Durable 2004" (ACI ECD009 BioCatOx) for financial support.

[1] B. Meunier, S. P. de Visser, S. Shaik, *Chem. Rev.* **2004**, *104*, 3947–3980.
[2] R. M. Burger, *Struct. Bonding (Berlin)* **2000**, *97*, 287–303.
[3] J. J. Girerd, F. Banse, A. J. Simaan, *Struct. Bonding (Berlin)* **2000**, *97*, 145–177.
[4] M. Costas, M. P. Mehn, M. P. Jensen, L. Que, Jr., *Chem. Rev.* **2004**, *104*, 939–986.
[5] H. Wada, S. Ogo, S. Nagatomo, T. Kitagawa, Y. Watanabe, K. Jitsukawa, H. Masuda, *Inorg. Chem.* **2002**, *41*, 616–618.
[6] T. Kitagawa, A. Dey, P. Lugo-Mas, J. B. Benedict, W. Kaminsky, E. Solomon, J. A. Kovacs, *J. Am. Chem. Soc.* **2006**, *128*, 14448–14449.
[7] R. Y. N. Ho, G. Roelfes, B. L. Feringa, L. Que, Jr., *J. Am. Chem. Soc.* **1999**, *121*, 264–265.
[8] A. J. Simaan, S. Dopner, F. Banse, S. Bourcier, G. Bouchoux, A. Boussac, P. Hildebrandt, J. J. Girerd, *Eur. J. Inorg. Chem.* **2000**, 1627–1633.
[9] J. S. Griffith, *The Theory of Transition Metal Ions*, Cambridge University Press, London, **1961**.
[10] C. P. S. Taylor, *Biochim. Biophys. Acta.* **1977**, *491*, 137–149.
[11] P. J. Alonso, J. I. Martinez, I. Garcia-Rubio, *Coord. Chem. Rev.* **2007**, *251*, 12–24.
[12] B. R. McGarvey, *Coord. Chem. Rev.* **1998**, *170*, 75–92.
[13] B. R. McGarvey, *Quim. Nova* **1998**, *21*, 206–213.
[14] A. J. Simaan, F. Banse, P. Mialane, A. Boussac, S. Un, T. Kargar-Grisel, G. Bouchoux, J. J. Girerd, *Eur. J. Inorg. Chem.* **1999**, 993–996.
[15] M. Martinho, F. Banse, J. Sainton, C. Philouze, R. Guillot, G. Blain, P. Dorlet, S. Lecomte, J. J. Girerd, *Inorg. Chem.* **2007**, *46*, 1709–1717.
[16] F. Neese, J. M. Zaleski, K. L. Zaleski, E. I. Solomon, *J. Am. Chem. Soc.* **2000**, *122*, 11703–11724.
[17] G. Roelfes, V. Vrajmasu, K. Chen, R. Y. N. Ho, J. U. Rohde, C. Zondervan, R. M. la Crois, E. P. Schudde, M. Lutz, A. L. Spek, R. Hage, B. L. Feringa, E. Munck, L. Que, Jr., *Inorg. Chem.* **2003**, *42*, 2639–2653.
[18] M. E. deVries, R. M. La Crois, G. Roelfes, H. Kooijman, A. L. Spek, R. Hage, B. L. Feringa, *Chem. Commun.* **1997**, 1549–1550.
[19] O. Horner, C. Jeandey, J. L. Oddou, P. Bonville, C. J. McKenzie, J. M. Latour, *Eur. J. Inorg. Chem.* **2002**, 3278–3283.
[20] C. Kim, K. Chen, J. Kim, L. Que, Jr., *J. Am. Chem. Soc.* **1997**, *119*, 5964–5965.
[21] M. R. Bukowski, P. Comba, C. Limberg, M. Merz, L. Que, Jr., T. Wistuba, *Angew. Chem.* **2004**, *116*, 1303–1307; *Angew. Chem. Int. Ed.* **2004**, *43*, 1283–1287.
[22] We thank one of the reviewers for this suggestion.
[23] G. R. Hanson, K. E. Gates, C. J. Noble, M. Griffin, A. Mitchell, S. Benson, *J. Inorg. Biochem.* **2004**, *98*, 903–916.
[24] I. Bernal, I. M. Jensen, K. B. Jensen, C. J. McKenzie, H. Toftlund, J. P. Tuchagues, *J. Chem. Soc. Dalton Trans.* **1995**, 3667–3675.

Received: October 9, 2007
Published online: January 31, 2008

